EUROPEAN ORGANIZATION FOR NUCLEAR RESEARCH

CERN-EP/2001-008
26 January 2001

Study of the $e^+e^- \rightarrow Z\gamma\gamma \rightarrow q\bar{q}\gamma\gamma$ Process at LEP

The L3 Collaboration

Abstract

The process $e^+e^- \rightarrow Z\gamma\gamma \rightarrow q\bar{q}\gamma\gamma$ is studied in $0.5\,\mathrm{fb}^{-1}$ of data collected with the L3 detector at centre-of-mass energies between 130.1 GeV and 201.7 GeV. Cross sections are measured and found to be consistent with the Standard Model expectations. The study of the least energetic photon constrains the quartic gauge boson couplings to $-0.008\ \mathrm{GeV}^{-2} < a_0/\Lambda^2 < 0.005\ \mathrm{GeV}^{-2}$ and $-0.007\ \mathrm{GeV}^{-2} < a_c/\Lambda^2 < 0.011\ \mathrm{GeV}^{-2}$, at 95% confidence level.

Submitted to *Phys. Lett. B*

1 Introduction

The LEP data offer new insight into the Standard Model of electroweak interactions [1] by investigating the production of three gauge bosons. Results were recently reported on studies of the reactions $e^+e^- \rightarrow Z\gamma\gamma$ [2] and $e^+e^- \rightarrow W^+W^-\gamma$ [3,4]. This letter describes the extension of the study of the $e^+e^- \rightarrow Z\gamma\gamma$ process to centre-of-mass energies, $\sqrt{s}$, between 130 and 202 GeV. Final states with hadrons and isolated photons are considered to select $Z\gamma\gamma \rightarrow q\bar{q}\gamma\gamma$ events.

In the Standard Model, the $e^+e^- \rightarrow Z\gamma\gamma$ process occurs via radiation of photons from the incoming electron and/or positron. One possible diagram is presented in Figure 1a.

The $e^+e^- \rightarrow Z\gamma\gamma$ signal is defined by phase-space requirements on the energies E_γ and angles θ_γ of the two photons, and on the propagator mass $\sqrt{s'}$:

$$E_\gamma > 5 \text{ GeV} \tag{1}$$

$$|\cos\theta_\gamma| < 0.97 \tag{2}$$

$$|\sqrt{s'} - m_Z| < 2\Gamma_Z \tag{3}$$

where m_Z and Γ_Z are the Z boson mass and width. In the following, hadronic decays of the Z boson are considered. Events with hadrons and initial state photons falling outside the signal definition cuts are referred to as "non-resonant" background.

A single initial state radiation photon can also lower the effective centre-of-mass energy of the e^+e^- collision to m_Z, with the subsequent production of a quark-antiquark pair. This photon can be mistaken for the most energetic photon of the $e^+e^- \rightarrow Z\gamma\gamma \rightarrow q\bar{q}\gamma\gamma$ process. Two sources can then mimic the least energetic photon: either the direct radiation of photons from the quarks or photons originating from hadronic decays, misidentified electrons or unresolved π^0s. These background processes are depicted in Figures 1b and 1c, respectively.

In order to compare experimental results with $e^+e^- \rightarrow q\bar{q}\gamma\gamma$ matrix element calculations, a further requirement is applied on the angle $\theta_{\gamma q}$ between the photons and the nearest quark:

$$\cos\theta_{\gamma q} < 0.98. \tag{4}$$

This cut avoids collinear divergences. Its inclusion makes the signal definition used here different from the previous one [2]. Signal cross sections calculated with the KK2f Monte Carlo program [5] range from 0.9 pb at $\sqrt{s} = 130.1$ GeV down to 0.3 pb at $\sqrt{s} = 201.7$ GeV.

The $Z\gamma\gamma$ final state could also originate from the s-channel exchange of a Z boson, as presented in Figure 1d. This process is forbidden at tree level in the Standard Model, but it is expected to occur in the presence of Quartic Gauge boson Couplings (QGC) beyond the Standard Model.

2 Data and Monte Carlo Samples

This measurement uses data collected with the L3 detector [6] at LEP in the years from 1995 through 1999, at centre-of-mass energies between $\sqrt{s} = 130.1$ GeV and $\sqrt{s} = 201.7$ GeV, for a total integrated luminosity of 0.5 fb^{-1}. The centre-of-mass energies and the corresponding integrated luminosities are listed in Table 1. Given their relatively low luminosities, the $\sqrt{s} =$ 130.1 GeV and $\sqrt{s} = 136.1$ GeV data sample are combined into a single luminosity averaged sample at $\sqrt{s} = 133.1$ GeV. Similarly the $\sqrt{s} = 161.3$ GeV and $\sqrt{s} = 172.3$ GeV samples are merged into a single sample at $\sqrt{s} = 166.8$ GeV.

The KK2f Monte Carlo program is used to generate $e^+e^- \rightarrow q\bar{q}(\gamma\gamma)$ events, that are assigned to the signal or the background according to the criteria (1)−(4). The hadronisation process is simulated with the JETSET [7] program. Other background processes are generated with the Monte Carlo programs PYTHIA [7] ($e^+e^- \rightarrow Ze^+e^-$ and $e^+e^- \rightarrow ZZ$), KORALZ [8] ($e^+e^- \rightarrow \tau^+\tau^-(\gamma)$), PHOJET [9] ($e^+e^- \rightarrow e^+e^-$ hadrons) and KORALW [10] for W^+W^- production except for the $e\nu_e q\bar{q}'$ final states, generated with EXCALIBUR [11].

The L3 detector response is simulated using the GEANT [12] and GHEISHA [13] programs, which model the effects of energy loss, multiple scattering and showering in the detector. Time dependent detector inefficiencies, as monitored during data taking periods, are also simulated.

$\sqrt{s}$ (GeV)	Integrated Luminosity (pb^{-1})
133.1	12.0
166.8	21.1
182.7	55.3
188.7	176.3
191.6	29.4
195.5	83.7
199.5	82.8
201.7	37.0

Table 1: Average centre-of-mass energies and corresponding integrated luminosities of the data samples used for this analysis.

3 Event Selection

The $e^+e^- \rightarrow Z\gamma\gamma \rightarrow q\bar{q}\gamma\gamma$ selection demands balanced hadronic events with two isolated photons and small energy deposition at low polar angle. Selection criteria on photon energies and angles follow directly from the signal definition as $E_\gamma > 5$ GeV and $|\cos\theta_\gamma| < 0.97$. The invariant mass $M_{q\bar{q}}$ of the reconstructed hadronic system, forced into two jets using the DURHAM algorithm [14], is required to be consistent with a Z boson decaying into hadrons, 72 GeV $< M_{q\bar{q}} <$ 116 GeV.

The main background after these requirements is due to the "non-resonant" production of two photons and a hadronic system. The relativistic velocity $\beta_Z = p_Z/E_Z$ of the system recoiling against the photons, calculated assuming its mass to be the nominal Z mass, is larger for part of these background events than for the signal and an upper cut is used to reject those events. It is optimised for each centre-of-mass energy, as listed in Table 2.

Other classes of background events, shown in Figure 1b and Figure 1c, are rejected by an upper bound on the energy $E_{\gamma 1}$ of the most energetic photon. This requirement, presented in Table 2, suppresses the resonant return to the Z, whose photons are harder than the signal ones. A lower bound of 17° on the angle ω between the least energetic photon and the closest jet is also imposed. This requirement is more restrictive than the similar cut on $\cos\theta_{\gamma q}$ included in the signal definition. Data and Monte Carlo distributions of the selection variables are presented in Figure 2 for the data collected at $\sqrt{s} = 192$ GeV-202 GeV when selection criteria on all the other variables are applied. Good agreement between data and Monte Carlo is observed.

$\sqrt{s}$ (GeV)	133.1	166.8	182.7	188.7	191.6	195.5	199.6	201.7
$\beta_{\mathrm{Z}} <$	0.48	0.61	0.64	0.66	0.66	0.67	0.69	0.70
E_{γ_1}(GeV) $<$	31.9	55.0	67.6	69.8	72.8	74.2	75.8	76.6

Table 2: Energy dependent criteria for the selection of $\mathrm{e^+e^-} \rightarrow \mathrm{Z}\gamma\gamma \rightarrow \mathrm{q\bar{q}}\gamma\gamma$ events.

4 Results

The signal efficiencies and the numbers of events selected in the data and Monte Carlo samples are summarised in Table 3. The dominant background is hadronic events with photons. About half of these are "non-resonant" events. In the remaining cases, they originate either from final state radiation or are fake photons.

A clear signal structure is observed in the spectra of the recoil mass to the two photons, as presented in Figure 3 for the $\sqrt{s} = 192$ GeV $-$ 202 GeV data sample and for the total one. The $\mathrm{e^+e^-} \rightarrow \mathrm{Z}\gamma\gamma \rightarrow \mathrm{q\bar{q}}\gamma\gamma$ cross sections, σ, are determined from a fit to the corresponding spectra at each $\sqrt{s}$. Background predictions are fixed in the fit. The results are listed in Table 4 with their statistical and systematic uncertainties. The systematic uncertainties on the cross section measurement are of the order of 10% [2]. The main contributions arise from the signal and background Monte Carlo statistics (6%) and a variation of $\pm 2\%$ of the energy scale of the hadronic calorimeter (6%). A variation of $\pm 0.5\%$ of the energy scale of the electromagnetic calorimeter does not yield sizable effects. Other sources of systematic uncertainties are the selection procedure (3%) and the background normalisation (3%). The latter is estimated by varying by 10% the normalisation of the "non-resonant" background, as estimated from a comparison between the KK2f and PYTHIA Monte Carlo predictions for hadronic events with photons, and by 20% that of the other backgrounds. Uncertainties on the determination of the integrated luminosity are negligible.

The measurements are in good agreement with the theoretical predictions σ^{SM}, as calculated with the KK2f Monte Carlo program, listed in Table 4. The error on the predictions (1.5%) is the quadratic sum of the theory uncertainty [5] and the statistical uncertainty of the Monte Carlo sample generated for the calculation. These results are presented in Figure 4 together with the expected evolution with $\sqrt{s}$ of the Standard Model cross section.

The distribution of the recoil mass to the two photons for the full data sample, presented in Figure 3b, is fitted to calculate the ratio $R_{\mathrm{Z}\gamma\gamma}$ between all the observed data and the signal expectation. The background predictions are fixed in the fit, which yields:

$$R_{\mathrm{Z}\gamma\gamma} = \frac{\sigma}{\sigma^{\mathrm{SM}}} = 0.85 \pm 0.11 \pm 0.06$$

in agreement with the Standard Model. The first uncertainty is statistical while the second is systematic. The correlation of the energy scale and background normalisation uncertainties between data samples is taken into account.

$\sqrt{s}$(GeV)	ε(%)	Data	Monte Carlo	N_s	$N_b^{\mathrm{q\bar{q}}}$	N_b^{Other}
133.1	45	4	5.9 ± 0.5	5.0 ± 0.5	0.8 ± 0.2	0.08 ± 0.02
166.8	52	4	6.7 ± 0.3	4.9 ± 0.3	1.4 ± 0.1	0.4 ± 0.1
182.7	51	13	13.6 ± 0.7	10.8 ± 0.6	2.7 ± 0.2	0.06 ± 0.02
188.7	52	38	40.3 ± 2.0	32.5 ± 1.7	7.2 ± 1.1	0.6 ± 0.1
191.6	42	2	5.9 ± 0.4	4.1 ± 0.3	1.8 ± 0.3	0.06 ± 0.02
195.5	46	13	17.5 ± 0.9	12.4 ± 0.7	4.9 ± 0.5	0.2 ± 0.1
199.6	46	14	15.0 ± 0.8	11.5 ± 0.6	3.4 ± 0.5	0.13 ± 0.05
201.7	48	9	6.9 ± 0.5	5.2 ± 0.4	1.7 ± 0.3	0.06 ± 0.02

Table 3: Yields of the $\mathrm{e^+e^-} \to \mathrm{Z}\gamma\gamma \to \mathrm{q\bar{q}}\gamma\gamma$ selection. The signal efficiencies ε are given, together with the observed and expected numbers of events. The right half of the table details the composition of the Monte Carlo samples with N_s denoting the signal, $N_b^{\mathrm{q\bar{q}}}$ the $\mathrm{q\bar{q}}$ and N_b^{Other} the other backgrounds. The uncertainties are statistical only.

$\sqrt{s}$ (GeV)	σ (pb)	σ^{SM} (pb)
133.1	$0.70 \pm 0.40 \pm 0.07$	0.923 ± 0.012
166.8	$0.17 \pm 0.13 \pm 0.02$	0.475 ± 0.006
182.7	$0.36 \pm 0.13 \pm 0.04$	0.379 ± 0.004
188.7	$0.34 \pm 0.06 \pm 0.03$	0.350 ± 0.004
191.6	$0.09 \pm 0.09 \pm 0.01$	0.326 ± 0.004
195.5	$0.30 \pm 0.11 \pm 0.03$	0.321 ± 0.004
199.6	$0.28 \pm 0.11 \pm 0.03$	0.304 ± 0.004
201.7	$0.50 \pm 0.18 \pm 0.05$	0.296 ± 0.003

Table 4: Results of the measurements of the $\mathrm{e^+e^-} \to \mathrm{Z}\gamma\gamma \to \mathrm{q\bar{q}}\gamma\gamma$ cross section, σ, with statistical and systematic uncertainties. The predicted values of cross sections, σ^{SM}, are also listed.

5 Study of Quartic Gauge Boson Couplings

The contribution of anomalous QGCs to $\mathrm{Z}\gamma\gamma$ production is described by two additional dimension-six terms in the electroweak Lagrangian [15, 16]:

$$\begin{aligned}
\mathcal{L}_6^0 &= -\frac{\pi\alpha}{4\Lambda^2} a_0 F_{\mu\nu} F^{\mu\nu} \vec{W}_\rho \cdot \vec{W}^\rho \\
\mathcal{L}_6^c &= -\frac{\pi\alpha}{4\Lambda^2} a_c F_{\mu\rho} F^{\mu\sigma} \vec{W}^\rho \cdot \vec{W}_\sigma,
\end{aligned}$$

where α is the fine structure constant, $F_{\mu\nu}$ is the field strength tensor of the photon and $\vec{W}_\sigma$ is the weak boson field. The parameters a_0 and a_c describe the strength of the QGCs and Λ represents the unknown scale of the New Physics responsible for the anomalous contributions. In the Standard Model, $a_0 = a_c = 0$. A more detailed description of QGCs has recently appeared [17]. Indirect limits on QGCs were derived from precision measurements at the Z pole [18].

Anomalous values of QGCs are expected to manifest themselves via deviations in the total $\mathrm{e^+e^-} \to \mathrm{Z}\gamma\gamma$ cross section, as presented in Figure 4. In the Standard Model, $\mathrm{Z}\gamma\gamma$ production occurs via bremsstrahlung with the low energy photon preferentially produced close to the beam direction. The QGC s-channel production results instead in a harder energy spectrum and a more central angular distribution of the least energetic photon [16]. Distributions for this photon of the reconstructed energy, the cosine of the polar angle and the transverse momentum for the full data sample are compared in Figure 5 with the predictions from signal and background Monte Carlo. Predictions in the case of a non zero value of a_0/Λ^2 or a_c/Λ^2 are also shown. They are obtained by reweighting [2] the Standard Model signal Monte Carlo events with an analytical calculation of the QGC matrix element [16]. Monte Carlo studies indicate the transverse momentum as the most sensitive distribution to possible anomalous QGC contributions. A fit to this distribution is performed for each data sample, leaving one of the two QGCs free at a time and fixing the other to zero. It yields the 68% confidence level results:

$$a_0/\Lambda^2 = -0.002^{+0.003}_{-0.002}\ \mathrm{GeV}^{-2} \ \text{ and } \ a_c/\Lambda^2 = -0.001^{+0.006}_{-0.004}\ \mathrm{GeV}^{-2}\,,$$

in agreement with the expected Standard Model values of zero. A simultaneous fit to both the parameters gives the 95% confidence level limits:

$$-0.008\ \mathrm{GeV}^{-2} < a_0/\Lambda^2 < 0.005\ \mathrm{GeV}^{-2} \ \text{ and } \ -0.007\ \mathrm{GeV}^{-2} < a_c/\Lambda^2 < 0.011\ \mathrm{GeV}^{-2}\,,$$

as shown in Figure 6. A correlation coefficient of −57% is observed. The experimental systematic uncertainties and those on the Standard Model $\mathrm{e^+e^-} \rightarrow \mathrm{Z}\gamma\gamma \rightarrow \mathrm{q\bar{q}}\gamma\gamma$ cross section predictions are taken into account in the fit.

Acknowledgements

We wish to express our gratitude to the CERN accelerator divisions for the superb performance and the continuous and successful upgrade of the LEP machine. We acknowledge the contributions of the engineers and technicians who have participated in the construction and maintenance of this experiment.

Appendix

To allow the combination of our results with those of the other LEP experiments, the cross sections σ are also measured in the more restrictive phase space obtained by modifying the conditions (2) and (4) into $|\cos\theta_\gamma| < 0.95$ and $\cos\theta_{\gamma\mathrm{q}} < 0.9$, respectively. The results are:

$$\begin{aligned}
\sigma(182.7\ \mathrm{GeV}) &= 0.11 \pm 0.11 \pm 0.01\ \mathrm{pb} \quad (\mathrm{SM}: 0.233 \pm 0.003\ \mathrm{pb})\\
\sigma(188.7\ \mathrm{GeV}) &= 0.28 \pm 0.07 \pm 0.03\ \mathrm{pb} \quad (\mathrm{SM}: 0.214 \pm 0.003\ \mathrm{pb})\\
\sigma(194.5\ \mathrm{GeV}) &= 0.15 \pm 0.07 \pm 0.02\ \mathrm{pb} \quad (\mathrm{SM}: 0.197 \pm 0.003\ \mathrm{pb})\\
\sigma(200.2\ \mathrm{GeV}) &= 0.15 \pm 0.07 \pm 0.01\ \mathrm{pb} \quad (\mathrm{SM}: 0.185 \pm 0.003\ \mathrm{pb}).
\end{aligned}$$

The first uncertainty is statistical, the second systematic and the values in parentheses indicate the Standard Model predictions. The samples at $\sqrt{s} = 192$ GeV−196 GeV and $\sqrt{s} = 200$ GeV−202 GeV are respectively merged into the $\sqrt{s} = 194.5$ GeV and $\sqrt{s} = 200.2$ GeV ones.

References

[1] S. L. Glashow, Nucl. Phys. **22** (1961) 579; A. Salam, in Elementary Particle Theory, ed. N. Svartholm, (Almqvist and Wiksell, Stockholm, 1968), p. 367; S. Weinberg, Phys. Rev. Lett. **19** (1967) 1264.

[2] L3 Collab., M. Acciarri *et al.*, Phys. Lett. **B 478** (2000) 39.

[3] L3 Collab., M. Acciarri *et al.*, Phys. Lett. **B 490** (2000) 187.

[4] OPAL Collab., G. Abbiendi *et al.*, Phys. Lett. **B 471** (1999) 293.

[5] KK2f version 4.13 is used; S. Jadach, B.F.L. Ward and Z. Wąs, Comp. Phys. Comm **130** (2000) 260.

[6] L3 Collab., B. Adeva *et al.*, Nucl. Instr. and Meth. **A 289** (1990) 35; L3 Collab., O. Adriani *et al.*, Phys. Rep. **236** (1993) 1; I. C. Brock *et al.*, Nucl. Instr. and Meth. **A 381** (1996) 236; M. Chemarin *et al.*, Nucl. Instr. and Meth. **A 349** (1994) 345; M. Acciarri *et al.*, Nucl. Instr. and Meth. **A 351** (1994) 300; A. Adam *et al.*, Nucl. Instr. and Meth. **A 383** (1996) 342; G. Basti *et al.*, Nucl. Instr. and Meth. **A 374** (1996) 293.

[7] PYTHIA version 5.772 and JETSET version 7.4 are used; T. Sjöstrand, CERN–TH/7112/93 (1993), revised 1995; T. Sjöstrand, Comp. Phys. Comm. **82** (1994) 74.

[8] KORALZ version 4.03 is used; S. Jadach, B. F. L. Ward and Z. Wąs, Comp. Phys. Comm **79** (1994) 503.

[9] PHOJET version 1.05 is used; R. Engel, Z. Phys. **C 66** (1995) 203; R. Engel and J. Ranft, Phys. Rev. **D 54** (1996) 4244.

[10] KORALW version 1.33 is used; M. Skrzypek *et al.*, Comp. Phys. Comm. **94** (1996) 216; M. Skrzypek *et al.*, Phys. Lett. **B 372** (1996) 289.

[11] R. Kleiss and R. Pittau, Comp. Phys. Comm. **85** (1995) 447; R. Pittau, Phys. Lett. **B 335** (1994) 490.

[12] GEANT version 3.15 is used; R. Brun *et al.*, preprint CERN–DD/EE/84–1 (1984), revised 1987.

[13] H. Fesefeldt, report RWTH Aachen PITHA 85/02 (1985).

[14] S. Bethke *et al.*, Nucl. Phys. **B 370** (1992) 310.

[15] G. Bélanger and F. Boudjema, Phys. Lett. **B 288** (1992) 201.

[16] W. J. Stirling and A. Werthenbach, Phys. Lett. **C 14** (2000) 103.

[17] G. Bélanger *et al.*, Eur. Phys. J. **C 13** (2000) 283.

[18] A. Brunstein, O. J. P. Éboli and M. C. Gonzales-Garcia, Phys. Lett. **B 375** (1996) 233.

The L3 Collaboration:

M.Acciarri,[25] P.Achard,[19] O.Adriani,[16] M.Aguilar-Benitez,[24] J.Alcaraz,[24] G.Alemanni,[21] J.Allaby,[17] A.Aloisio,[27] M.G.Alviggi,[27] G.Ambrosi,[19] H.Anderhub,[47] V.P.Andreev,[6,32] T.Angelescu,[12] F.Anselmo,[9] A.Arefiev,[26] T.Azemoon,[3] T.Aziz,[10] P.Bagnaia,[37] A.Bajo,[24] L.Baksay,[42] A.Balandras,[4] S.V.Baldew,[2] S.Banerjee,[10] Sw.Banerjee,[4] A.Barczyk,[47,45] R.Barillère,[17] P.Bartalini,[21] M.Basile,[9] N.Batalova,[44] R.Battiston,[31] A.Bay,[21] F.Becattini,[16] U.Becker,[14] F.Behner,[47] L.Bellucci,[16] R.Berbeco,[3] J.Berdugo,[24] P.Berges,[14] B.Bertucci,[31] B.L.Betev,[47] S.Bhattacharya,[10] M.Biasini,[31] M.Biglietti,[27] A.Biland,[47] J.J.Blaising,[4] S.C.Blyth,[33] G.J.Bobbink,[2] A.Böhm,[1] L.Boldizsar,[13] B.Borgia,[37] D.Bourilkov,[47] M.Bourquin,[19] S.Braccini,[19] J.G.Branson,[39] F.Brochu,[4] A.Buffini,[16] A.Buijs,[43] J.D.Burger,[14] W.J.Burger,[31] X.D.Cai,[14] M.Capell,[14] G.Cara Romeo,[9] G.Carlino,[27] A.M.Cartacci,[16] J.Casaus,[24] G.Castellini,[16] F.Cavallari,[37] N.Cavallo,[34] C.Cecchi,[31] M.Cerrada,[24] F.Cesaroni,[22] M.Chamizo,[19] Y.H.Chang,[49] U.K.Chaturvedi,[18] M.Chemarin,[23] A.Chen,[49] G.Chen,[7] G.M.Chen,[7] H.F.Chen,[20] H.S.Chen,[7] G.Chiefari,[27] L.Cifarelli,[38] F.Cindolo,[9] C.Civinini,[16] I.Clare,[14] R.Clare,[36] G.Coignet,[4] N.Colino,[24] S.Costantini,[5] F.Cotorobai,[12] B.de la Cruz,[24] A.Csilling,[13] S.Cucciarelli,[31] T.S.Dai,[14] J.A.van Dalen,[29] R.D'Alessandro,[16] R.de Asmundis,[27] P.Déglon,[19] A.Degré,[4] K.Deiters,[45] D.della Volpe,[27] E.Delmeire,[19] P.Denes,[35] F.DeNotaristefani,[37] A.De Salvo,[47] M.Diemoz,[37] M.Dierckxsens,[2] D.van Dierendonck,[2] C.Dionisi,[37] M.Dittmar,[47] A.Dominguez,[39] A.Doria,[27] M.T.Dova,[18,♯] D.Duchesneau,[4] D.Dufournaud,[4] P.Duinker,[2] H.El Mamouni,[23] A.Engler,[33] F.J.Eppling,[14] F.C.Erné,[2] A.Ewers,[1] P.Extermann,[19] M.Fabre,[45] M.A.Falagan,[24] S.Falciano,[37,17] A.Favara,[17] J.Fay,[23] O.Fedin,[32] M.Felcini,[47] T.Ferguson,[33] H.Fesefeldt,[1] E.Fiandrini,[31] J.H.Field,[19] F.Filthaut,[17] P.H.Fisher,[14] I.Fisk,[39] G.Forconi,[14] K.Freudenreich,[47] C.Furetta,[25] Yu.Galaktionov,[26,14] S.N.Ganguli,[10] P.Garcia-Abia,[5] M.Gataullin,[30] S.S.Gau,[11] S.Gentile,[37,17] N.Gheordanescu,[12] S.Giagu,[37] Z.F.Gong,[20] G.Grenier,[23] O.Grimm,[47] M.W.Gruenewald,[8] M.Guida,[38] R.van Gulik,[2] V.K.Gupta,[35] A.Gurtu,[10] L.J.Gutay,[44] D.Haas,[5] A.Hasan,[28] D.Hatzifotiadou,[9] T.Hebbeker,[8] A.Hervé,[17] P.Hidas,[13] J.Hirschfelder,[33] H.Hofer,[47] G. Holzner,[47] H.Hoorani,[33] S.R.Hou,[49] Y.Hu,[29] I.Iashvili,[46] B.N.Jin,[7] L.W.Jones,[3] P.de Jong,[2] I.Josa-Mutuberría,[24] R.A.Khan,[18] D.Käfer,[1] M.Kaur,[18,◇] M.N.Kienzle-Focacci,[19] D.Kim,[37] J.K.Kim,[41] J.Kirkby,[17] D.Kiss,[13] W.Kittel,[29] A.Klimentov,[14,26] A.C.König,[29] M.Kopal,[44] A.Kopp,[46] V.Koutsenko,[14,26] M.Kräber,[47] R.W.Kraemer,[33] W.Krenz,[1] A.Krüger,[46] A.Kunin,[14,26] P.Ladron de Guevara,[24] I.Laktineh,[23] G.Landi,[16] M.Lebeau,[17] A.Lebedev,[14] P.Lebrun,[23] P.Lecomte,[47] P.Lecoq,[17] P.Le Coultre,[47] H.J.Lee,[8] J.M.Le Goff,[17] R.Leiste,[46] P.Levtchenko,[32] C.Li,[20] S.Likhoded,[46] C.H.Lin,[49] W.T.Lin,[49] F.L.Linde,[2] L.Lista,[27] Z.A.Liu,[7] W.Lohmann,[46] E.Longo,[37] Y.S.Lu,[7] K.Lübelsmeyer,[1] C.Luci,[17,37] D.Luckey,[14] L.Lugnier,[23] L.Luminari,[37] W.Lustermann,[47] W.G.Ma,[20] M.Maity,[10] L.Malgeri,[19] A.Malinin,[17] C.Maña,[24] D.Mangeol,[29] J.Mans,[35] G.Marian,[15] J.P.Martin,[23] F.Marzano,[37] K.Mazumdar,[10] R.R.McNeil,[6] S.Mele,[17] L.Merola,[27] M.Meschini,[16] W.J.Metzger,[29] M.von der Mey,[1] A.Mihul,[12] H.Milcent,[17] G.Mirabelli,[37] J.Mnich,[1] G.B.Mohanty,[10] T.Moulik,[10] G.S.Muanza,[23] A.J.M.Muijs,[2] B.Musicar,[39] M.Musy,[37] M.Napolitano,[27] F.Nessi-Tedaldi,[47] H.Newman,[30] T.Niessen,[1] A.Nisati,[37] H.Nowak,[46] R.Ofierzynski,[47] G.Organtini,[37] A.Oulianov,[26] C.Palomares,[24] D.Pandoulas,[1] S.Paoletti,[37,17] P.Paolucci,[27] R.Paramatti,[37] H.K.Park,[33] I.H.Park,[41] G.Passaleva,[17] S.Patricelli,[27] T.Paul,[11] M.Pauluzzi,[31] C.Paus,[17] F.Pauss,[47] M.Pedace,[37] S.Pensotti,[25] D.Perret-Gallix,[4] B.Petersen,[29] D.Piccolo,[27] F.Pierella,[9] M.Pieri,[16] P.A.Piroué,[35] E.Pistolesi,[25] V.Plyaskin,[26] M.Pohl,[19] V.Pojidaev,[26,16] H.Postema,[14] J.Pothier,[17] D.O.Prokofiev,[44] D.Prokofiev,[32] J.Quartieri,[38] G.Rahal-Callot,[47,17] M.A.Rahaman,[10] P.Raics,[15] N.Raja,[10] R.Ramelli,[47] P.G.Rancoita,[25] R.Ranieri,[16] A.Raspereza,[46] G.Raven,[39] P.Razis,[28] D.Ren,[47] M.Rescigno,[37] S.Reucroft,[11] S.Riemann,[46] K.Riles,[3] J.Rodin,[42] B.P.Roe,[3] L.Romero,[24] A.Rosca,[8] S.Rosier-Lees,[4] S.Roth,[1] C.Rosenbleck,[1] B.Roux,[29] J.A.Rubio,[17] G.Ruggiero,[16] H.Rykaczewski,[47] S.Saremi,[6] S.Sarkar,[37] J.Salicio,[17] E.Sanchez,[17] M.P.Sanders,[29] C.Schäfer,[17] V.Schegelsky,[32] S.Schmidt-Kaerst,[1] D.Schmitz,[1] H.Schopper,[48] D.J.Schotanus,[29] G.Schwering,[1] C.Sciacca,[27] A.Seganti,[9] L.Servoli,[31] S.Shevchenko,[30] N.Shivarov,[40] V.Shoutko,[26] E.Shumilov,[26] A.Shvorob,[30] T.Siedenburg,[1] D.Son,[41] B.Smith,[33] P.Spillantini,[16] M.Steuer,[14] D.P.Stickland,[35] A.Stone,[6] B.Stoyanov,[40] A.Straessner,[17] K.Sudhakar,[10] G.Sultanov,[18] L.Z.Sun,[20] S.Sushkov,[8] H.Suter,[47] J.D.Swain,[18] Z.Szillasi,[42,¶] T.Sztaricskai,[42,¶] X.W.Tang,[7] L.Tauscher,[5] L.Taylor,[11] B.Tellili,[23] D.Teyssier,[23] C.Timmermans,[29] Samuel C.C.Ting,[14] S.M.Ting,[14] S.C.Tonwar,[10] J.Tóth,[13] C.Tully,[17] K.L.Tung,[7] Y.Uchida,[14] J.Ulbricht,[47] E.Valente,[37] G.Vesztergombi,[13] I.Vetlitsky,[26] D.Vicinanza,[38] G.Viertel,[47] S.Villa,[36] M.Vivargent,[4] S.Vlachos,[5] I.Vodopianov,[32] H.Vogel,[33] H.Vogt,[46] I.Vorobiev,[33] A.A.Vorobyov,[32] A.Vorvolakos,[28] M.Wadhwa,[5] W.Wallraff,[1] M.Wang,[14] X.L.Wang,[20] Z.M.Wang,[20] A.Weber,[1] M.Weber,[1] P.Wienemann,[1] H.Wilkens,[29] S.X.Wu,[14] S.Wynhoff,[17] L.Xia,[30] Z.Z.Xu,[20] J.Yamamoto,[3] B.Z.Yang,[20] C.G.Yang,[7] H.J.Yang,[7] M.Yang,[7] J.B.Ye,[20] S.C.Yeh,[50] An.Zalite,[32] Yu.Zalite,[32] Z.P.Zhang,[20] G.Y.Zhu,[7] R.Y.Zhu,[30] A.Zichichi,[9,17,18] G.Zilizi,[42,¶] B.Zimmermann,[47] M.Zöller.[1]

1 I. Physikalisches Institut, RWTH, D-52056 Aachen, FRG[§]
III. Physikalisches Institut, RWTH, D-52056 Aachen, FRG[§]
2 National Institute for High Energy Physics, NIKHEF, and University of Amsterdam, NL-1009 DB Amsterdam, The Netherlands
3 University of Michigan, Ann Arbor, MI 48109, USA
4 Laboratoire d'Annecy-le-Vieux de Physique des Particules, LAPP,IN2P3-CNRS, BP 110, F-74941 Annecy-le-Vieux CEDEX, France
5 Institute of Physics, University of Basel, CH-4056 Basel, Switzerland
6 Louisiana State University, Baton Rouge, LA 70803, USA
7 Institute of High Energy Physics, IHEP, 100039 Beijing, China[△]
8 Humboldt University, D-10099 Berlin, FRG[§]
9 University of Bologna and INFN-Sezione di Bologna, I-40126 Bologna, Italy
10 Tata Institute of Fundamental Research, Bombay 400 005, India
11 Northeastern University, Boston, MA 02115, USA
12 Institute of Atomic Physics and University of Bucharest, R-76900 Bucharest, Romania
13 Central Research Institute for Physics of the Hungarian Academy of Sciences, H-1525 Budapest 114, Hungary[‡]
14 Massachusetts Institute of Technology, Cambridge, MA 02139, USA
15 KLTE-ATOMKI, H-4010 Debrecen, Hungary[¶]
16 INFN Sezione di Firenze and University of Florence, I-50125 Florence, Italy
17 European Laboratory for Particle Physics, CERN, CH-1211 Geneva 23, Switzerland
18 World Laboratory, FBLJA Project, CH-1211 Geneva 23, Switzerland
19 University of Geneva, CH-1211 Geneva 4, Switzerland
20 Chinese University of Science and Technology, USTC, Hefei, Anhui 230 029, China[△]
21 University of Lausanne, CH-1015 Lausanne, Switzerland
22 INFN-Sezione di Lecce and Università Degli Studi di Lecce, I-73100 Lecce, Italy
23 Institut de Physique Nucléaire de Lyon, IN2P3-CNRS,Université Claude Bernard, F-69622 Villeurbanne, France
24 Centro de Investigaciones Energéticas, Medioambientales y Tecnologícas, CIEMAT, E-28040 Madrid, Spain♭
25 INFN-Sezione di Milano, I-20133 Milan, Italy
26 Institute of Theoretical and Experimental Physics, ITEP, Moscow, Russia
27 INFN-Sezione di Napoli and University of Naples, I-80125 Naples, Italy
28 Department of Natural Sciences, University of Cyprus, Nicosia, Cyprus
29 University of Nijmegen and NIKHEF, NL-6525 ED Nijmegen, The Netherlands
30 California Institute of Technology, Pasadena, CA 91125, USA
31 INFN-Sezione di Perugia and Università Degli Studi di Perugia, I-06100 Perugia, Italy
32 Nuclear Physics Institute, St. Petersburg, Russia
33 Carnegie Mellon University, Pittsburgh, PA 15213, USA
34 INFN-Sezione di Napoli and University of Potenza, I-85100 Potenza, Italy
35 Princeton University, Princeton, NJ 08544, USA
36 University of Californa, Riverside, CA 92521, USA
37 INFN-Sezione di Roma and University of Rome, "La Sapienza", I-00185 Rome, Italy
38 University and INFN, Salerno, I-84100 Salerno, Italy
39 University of California, San Diego, CA 92093, USA
40 Bulgarian Academy of Sciences, Central Lab. of Mechatronics and Instrumentation, BU-1113 Sofia, Bulgaria
41 Laboratory of High Energy Physics, Kyungpook National University, 702-701 Taegu, Republic of Korea
42 University of Alabama, Tuscaloosa, AL 35486, USA
43 Utrecht University and NIKHEF, NL-3584 CB Utrecht, The Netherlands
44 Purdue University, West Lafayette, IN 47907, USA
45 Paul Scherrer Institut, PSI, CH-5232 Villigen, Switzerland
46 DESY, D-15738 Zeuthen, FRG
47 Eidgenössische Technische Hochschule, ETH Zürich, CH-8093 Zürich, Switzerland
48 University of Hamburg, D-22761 Hamburg, FRG
49 National Central University, Chung-Li, Taiwan, China
50 Department of Physics, National Tsing Hua University, Taiwan, China
§ Supported by the German Bundesministerium für Bildung, Wissenschaft, Forschung und Technologie
‡ Supported by the Hungarian OTKA fund under contract numbers T019181, F023259 and T024011.
¶ Also supported by the Hungarian OTKA fund under contract numbers T22238 and T026178.
♭ Supported also by the Comisión Interministerial de Ciencia y Tecnología.
♯ Also supported by CONICET and Universidad Nacional de La Plata, CC 67, 1900 La Plata, Argentina.
♢ Also supported by Panjab University, Chandigarh-160014, India.
△ Supported by the National Natural Science Foundation of China.

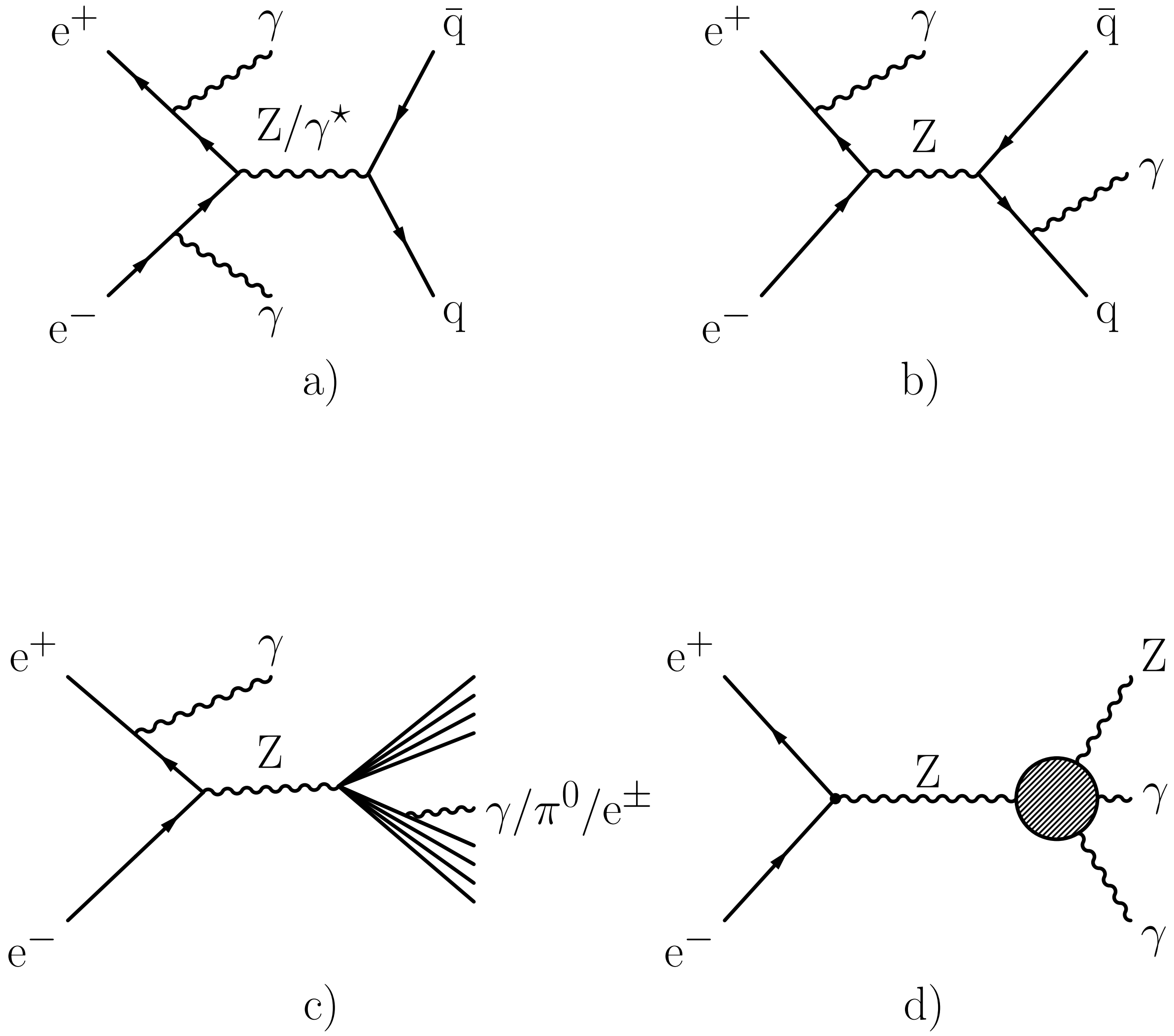

Figure 1: Diagrams of a) the Standard Model contribution to $e^+e^- \to Z\gamma\gamma$ signal and "non-resonant" background, b) the background from direct radiation of photon from the quarks, c) the background from photons, misidentified electrons or unresolved π^0s originating from hadrons and d) the anomalous QGC diagram.

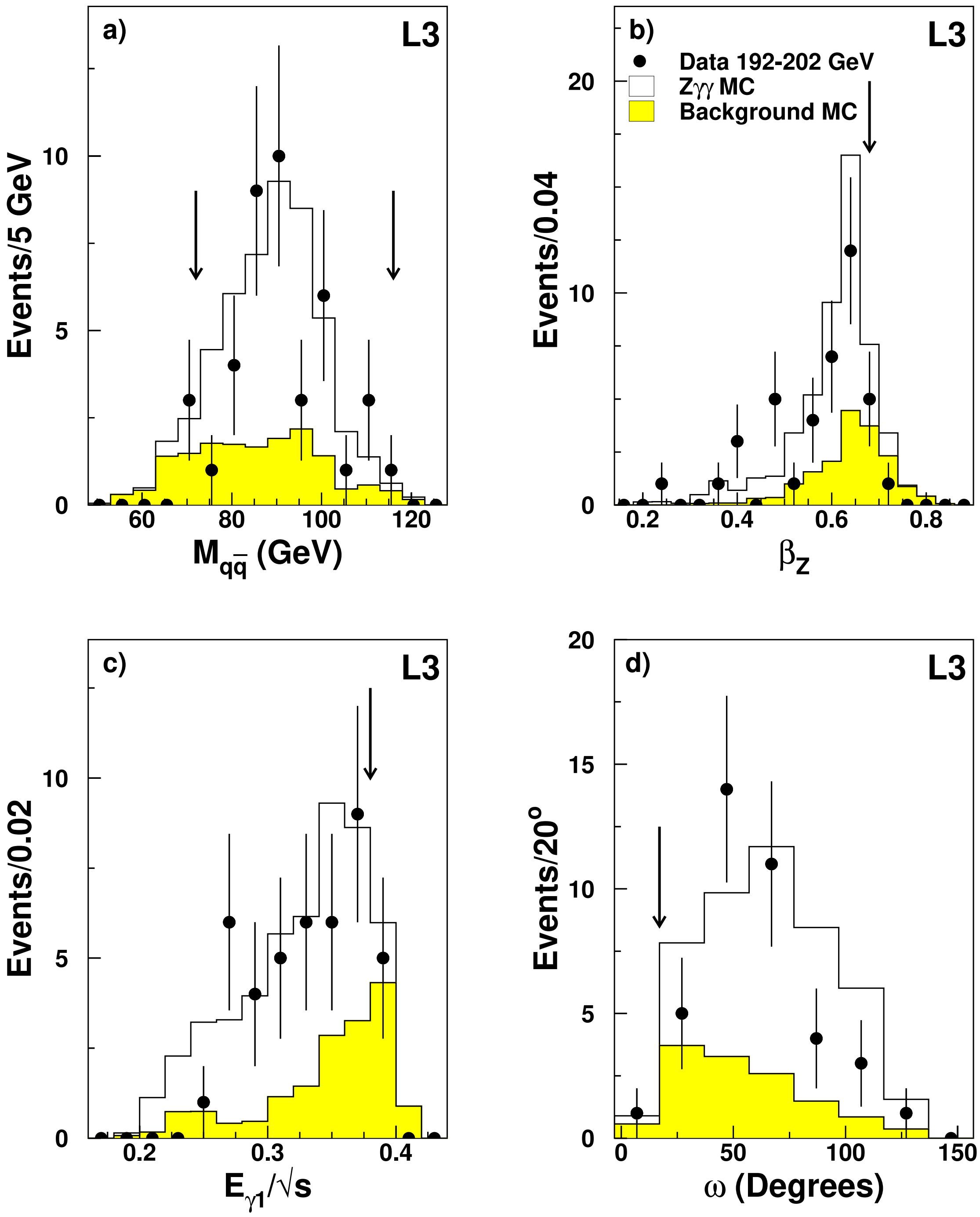

Figure 2: Distributions of a) the invariant mass $M_{q\bar{q}}$ of the hadronic system, b) the relativistic velocity β_Z of the reconstructed Z boson, c) the energy $E_{\gamma 1}$ of the most energetic photon and d) the angle ω between the least energetic photon and the nearest jet. Data, signal and background Monte Carlo samples are shown for $\sqrt{s}$ = 192 GeV – 202 GeV. The arrows show the position of the final selection requirements. In each plot, the selection criteria on the other variables are applied.

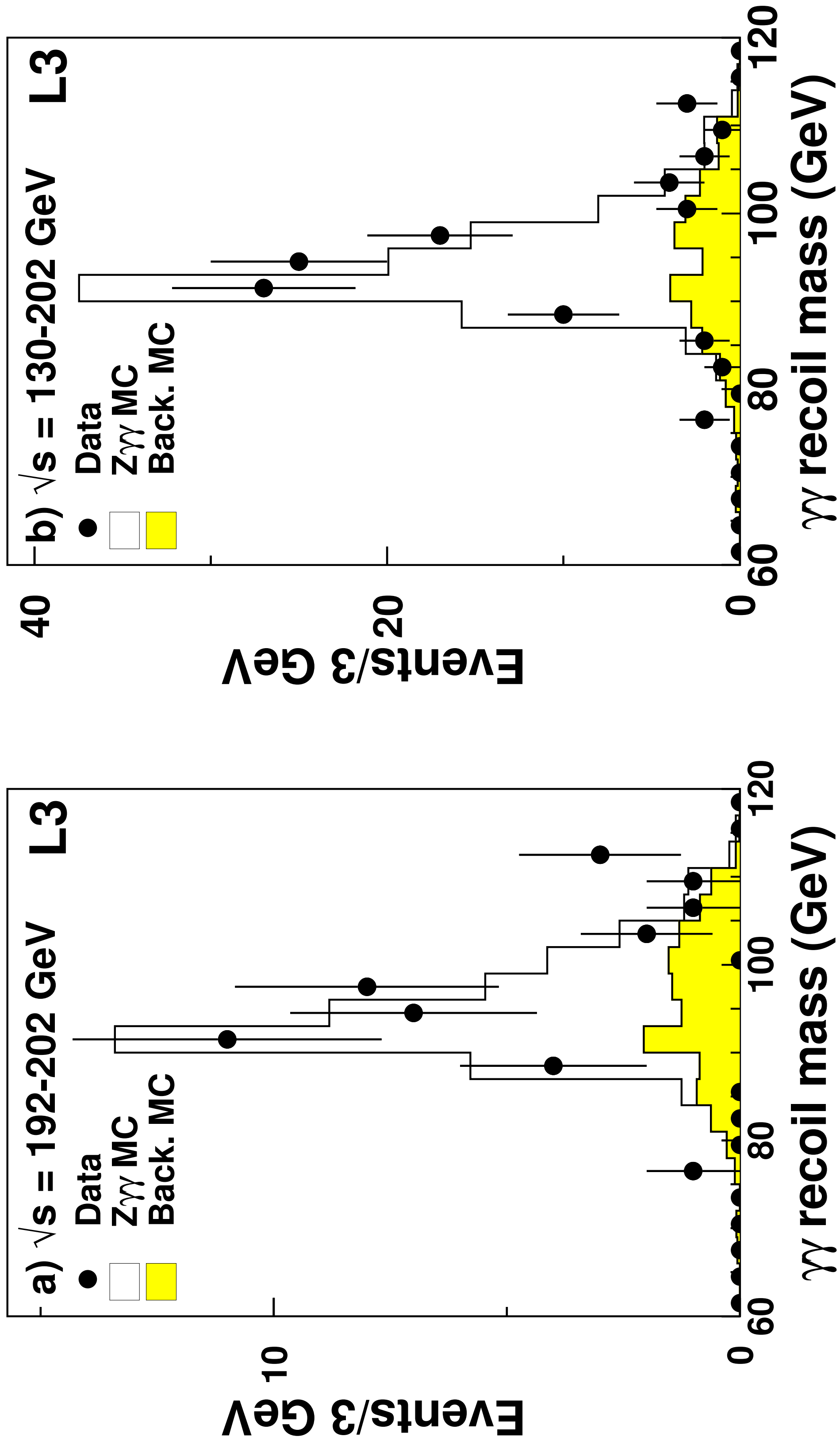

Figure 3: Recoil mass to the photon pairs in data, $Z\gamma\gamma$ and background Monte Carlo for a) $\sqrt{s} = 192$ GeV $- 202$ GeV and b) the total sample.

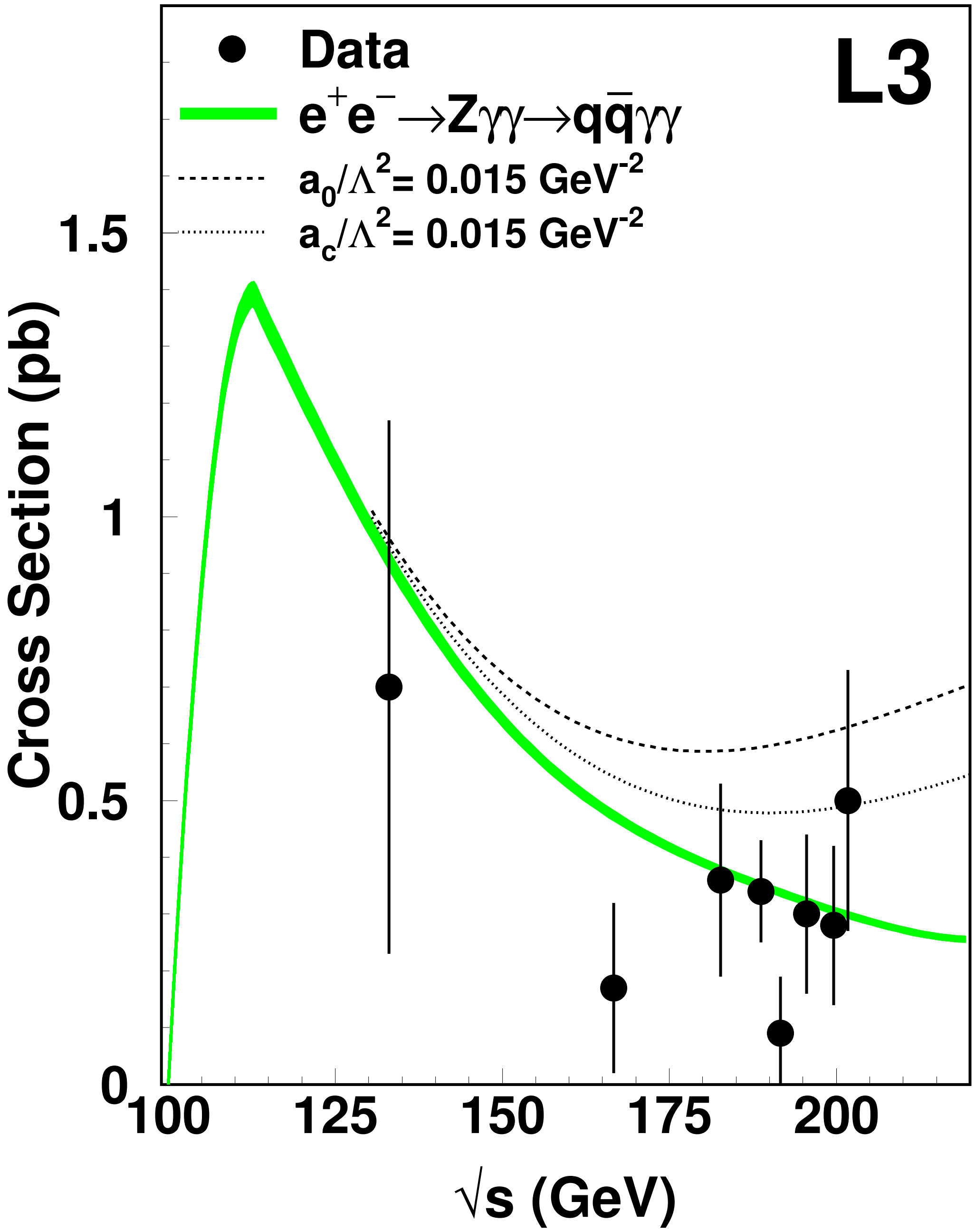

Figure 4: The cross section of the process $e^+e^- \to Z\gamma\gamma \to q\bar{q}\gamma\gamma$ as a function of the centre-of-mass energy. The signal is defined by the phase-space cuts of Equations (1)−(4). The width of the band corresponds to the Monte Carlo statistics and theory uncertainties. Dashed and dotted lines represent anomalous QGC predictions for $a_0/\Lambda^2 = 0.015$ GeV^{-2} and $a_c/\Lambda^2 = 0.015$ GeV^{-2}, respectively.

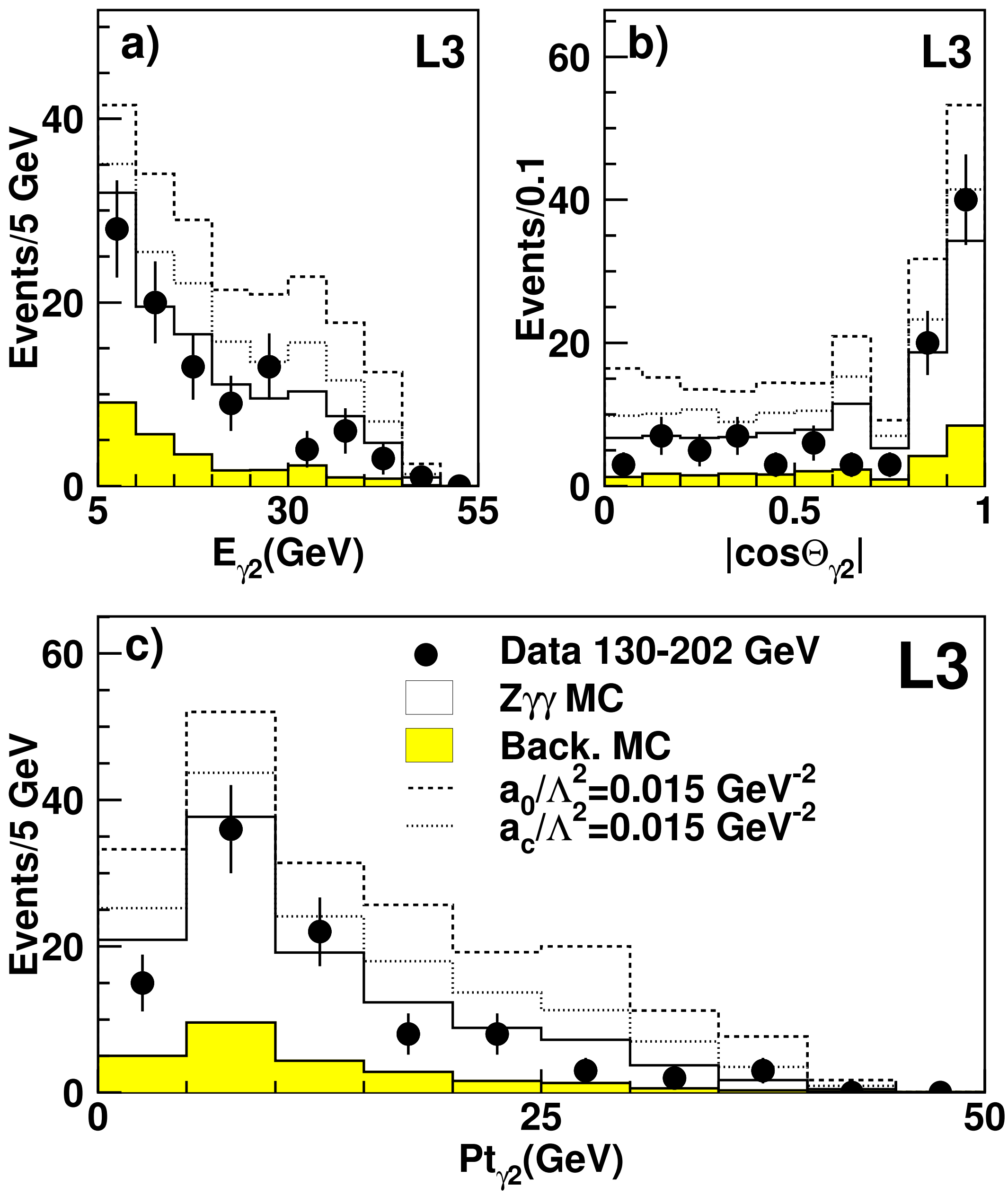

Figure 5: Distributions for the least energetic photon. a) the energy $E_{\gamma 2}$, b) the cosine of its polar angle $|\cos\theta_{\gamma 2}|$, c) its transverse momentum $Pt_{\gamma 2}$ with respect to the beam axis. Data, signal and background Monte Carlo are displayed for the full data sample together with QGC predictions.

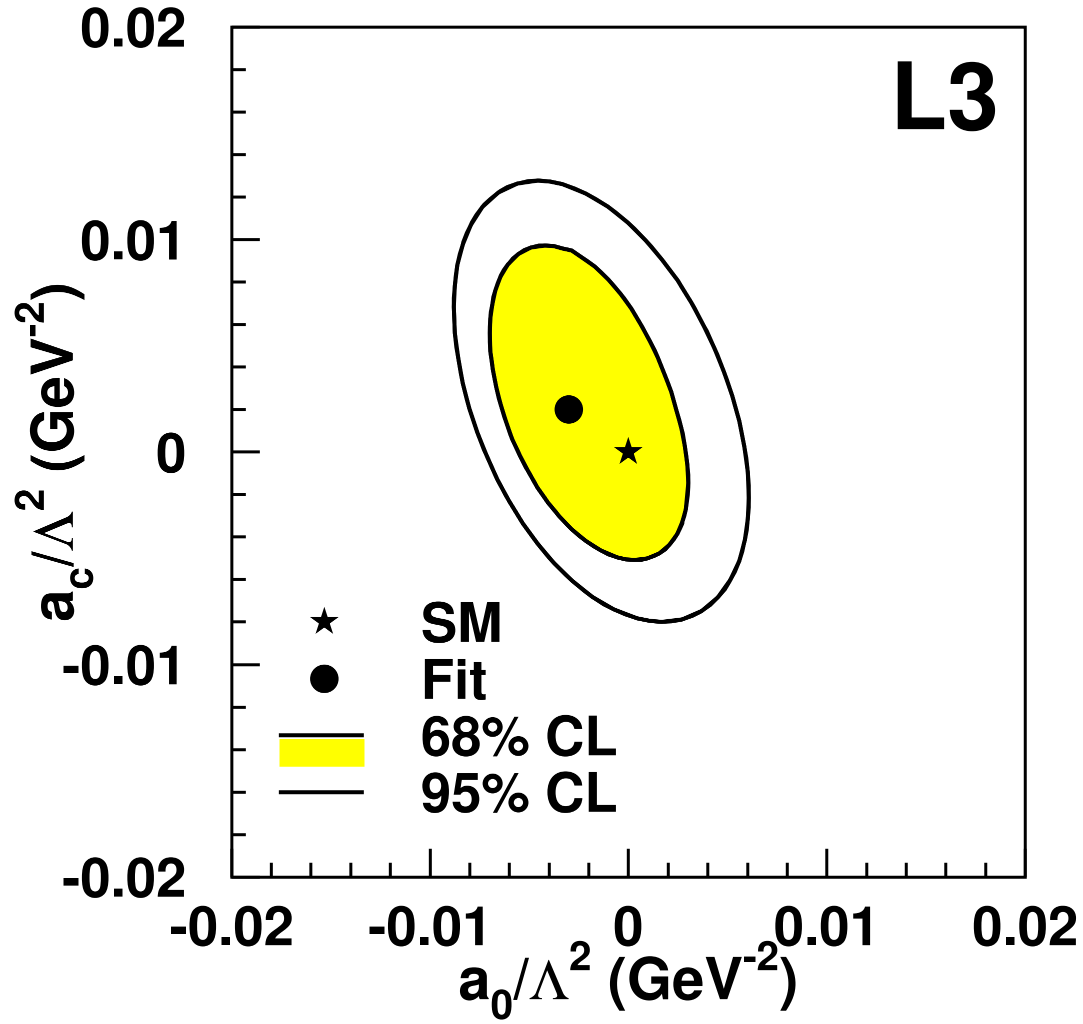

Figure 6: Two dimensional contours for the QGC parameters a_0/Λ^2 and a_c/Λ^2. The fit result is shown together with the Standard Model (SM) predictions.